Disrupted Thalamus White Matter Anatomy and Posterior Default Mode Network Effective Connectivity in Amnestic Mild Cognitive Impairment

Thomas Alderson[1], Elizabeth Kehoe[2], Liam Maguire[1], Dervla Farrell[2], Brian Lawlor[3], Rose Anne Kenny[3], Declan Lyons[4], Arun L.W. Bokde[2] and Damien Coyle[1*]

[1] Intelligent Systems Research Centre, University Ulster, Derry, UK.

[2] Trinity College Institute of Neuroscience and Cognitive Systems Group, Discipline of Psychiatry, School of Medicine, Trinity College Dublin, Dublin, Ireland.

[3] Mercer's Institute for Research on Ageing, St. James's Hospital, Dublin, Ireland and Trinity College Institute of Neuroscience, Trinity College Dublin, Dublin, Ireland.

[4] St. Patrick's Hospital, Steven's Lane, Dublin 8, Ireland.

* Correspondence:

Thomas Alderson, Intelligent Systems Research Centre, University Ulster, Magee Campus, Derry, UK

Email: thomashenryalderson@gmail.co.uk

Abstract

Alzheimer's disease (AD) and its prodromal state amnestic mild cognitive impairment (aMCI) are characterised by widespread abnormalities in inter-areal white matter fibre pathways and parallel disruption of default mode network (DMN) resting state functional and effective connectivity.

In healthy subjects, DMN and task positive network interaction are modulated by the thalamus suggesting that abnormal task-based DMN deactivation in aMCI may be a consequence of impaired thalamo-cortical white matter circuitry.

Thus, this paper uses a multimodal approach to assess white matter integrity between thalamus and DMN components and associated effective connectivity in healthy controls (HC) relative to aMCI patients.

Twenty-six HC and 20 older adults with aMCI underwent structural, functional and diffusion MRI scanning using the high angular resolution diffusion-weighted acquisition protocol. The DMN of each subject was identified using independent component analysis and resting state effective connectivity was calculated between thalamus and DMN nodes. White matter integrity changes between thalamus and DMN were investigated with constrained spherical deconvolution tractography.

Significant structural deficits in thalamic white matter projection fibres to posterior DMN components posterior cingulate cortex (PCC) and lateral inferior parietal lobe (IPL) were identified together with significantly reduced effective connectivity from left thalamus to left IPL. Crucially, impaired thalamo-cortical white matter circuitry correlated with memory performance. Disrupted thalamo-cortical structure was accompanied by significant reductions in IPL and PCC cortico-cortical effective connectivity. No structural deficits were found between DMN nodes.

Abnormal posterior DMN activity may be driven by changes in thalamic white matter connectivity; a view supported by the close anatomical and functional association of thalamic nuclei effected by AD pathology and the posterior DMN nodes.

We conclude that dysfunctional posterior DMN activity in aMCI is consistent with disrupted cortico-thalamo-cortical processing and thalamic-based dissemination of hippocampal disease agents to cortical hubs.

Keywords

Diffusion MRI, tractography, effective connectivity, Alzheimer's disease, mild cognitive impairment, default mode network, thalamus, resting state

1. Introduction

Alzheimer's disease (AD) is a chronic neurodegenerative disorder affecting approximately 6% of people over the age of 65 and accounting for 60 to 70% of dementia cases (Burns & Iliffe, 2009). Typically, the AD-prodromal stage presents as mild cognitive impairment (MCI; Stephan et al., 2012) clinically defined as cognitive difficulties beyond those expected based on age and education, but insufficient to interfere with daily activities (Petersen et al., 1999; Petersen, 2004). MCI can present with a variety of symptoms but is termed amnestic MCI (aMCI) in cases where memory loss is the predominant symptom.

In AD, the first neurofibrillary tangles appear in the parahippocampal regions (stage I) followed later, and accompanied by cognitive symptoms, in the hippocampus formation (stage III; Braak & Braak, 1991a, 1991b, 1995). Understandably, this knowledge has reinforced focus on the hippocampus in the context of memory loss in AD but much less well-known and less well-understood are the appearance of tangles and plaques in the thalamic nuclei in parallel with those in the hippocampus. Their appearance is often characterised as an event downstream of the hippocampus pathology transmitted by the projections of the mammillary bodies, but this view is challenged by metabolic studies indicating that the earliest consistent declines occur not in hippocampus but in posterior cingulate cortex (PCC; Minoshima, Foster, & Kuhl, 1994; Minoshima et al., 1997) where amyloid deposition is highest (Buckner et al., 2005; Mintun et al., 2006). The thalamus, with its dense network of reciprocal interconnections with both hippocampus and PCC, is therefore implicated by association (Vann, Aggleton, & Maguire, 2009; Aggleton et al., 2010).

Such a view is supported by detection of thalamic atrophy in pre-symptomatic familial AD on average 5.6 years prior to expected symptom onset (Ryan et al., 2013) together with increased amyloid burden (Knight et al., 2011) and substantial evidence suggesting that thalamic atrophy is present in MCI prior to AD (Chételat et al., 2005; Shiino et al., 2006; de Jong et al., 2008; Ferrarini et al., 2008; Cherubini et al., 2010; Roh et al., 2011; Pedro et al., 2012; Y. Zhang et al., 2013). Structural irregularities have a sufficient impact on thalamo-cortical circuits to allow healthy subjects to be differentiated from those with MCI through impaired functional integrity (Cantero et al., 2009). Conversely, carriers of the apolipoprotein ε2 allele i.e. those showing a genetic predisposition against developing AD, demonstrate significantly enhanced functional (Patel et al., 2013) and structural (Chiang, Zhan, Schuff, & Weiner, 2012) integrity of the thalamus.

Analysis of low frequency BOLD signal oscillations have revealed several resting state networks. Of these, the default mode network (DMN; (Raichle et al., 2001; Greicius, Krasnow, Reiss, & Menon, 2003; J S Damoiseaux et al., 2006) has consistently been identified as dysfunctional in both MCI and AD in the context of amyloid burden (Hedden et

al., 2009; Drzezga et al., 2011; Mormino et al., 2011; Sheline et al., 2011) and genetic risk (Roses, 1996; Sheline et al., 2010; L. Wang et al., 2012; Chhatwal et al., 2013).

The DMN comprises medial prefrontal cortex (mPFC), middle temporal gyrus (MTG), lateral inferior parietal lobes (IPL), PCC, and hippocampus regions. These nodes have been identified as important hubs within the cortex (Buckner et al., 2009) whose persistent background activity and dense, long range interconnectivity may facilitate the early deposition and prion-like transmission of amyloid plaques (Wermke, Sorg, Wohlschläger, & Drzezga, 2008; Raj, Kuceyeski, & Weiner, 2012). DMN topography is therefore recapitulated in the pattern of atrophy, hypometabolism and amyloid deposition within the cortex (Buckner et al., 2005; Buckner, Andrews-Hanna, & Schacter, 2008).

Thalamus appears to play a role modulating distributed cortical networks (Di & Biswal, 2014). It is therefore of note, that direct structural connections between the thalamus and DMN (or thalamo-DMN pathway) components have been described in vivo using diffusion tensor imaging (DTI; Fernández-Espejo et al., 2012) and that these are sites of atrophy (Zarei et al., 2010). Crucially, lesions to the thalamus are known to cause DMN dysfunction (D. T. Jones, Mateen, Lucchinetti, Jack, & Welker, 2011). One suggestion is that abnormal task-induced deactivation of DMN response patterns in aMCI are a consequence of impaired thalamo-cortical signalling (Pihlajamäki & Sperling, 2009).

The thalamus sends widespread connections to its ipsilateral cortical hemisphere which are returned via cortico-thalamic feedback connections. Together these form a thalamo-cortico-thalamic feedback loop (Sherman & Guillery, 2006; Murray Sherman, 2007; Zhang et al., 2008; Zhang, Snyder, Shimony, Fox, & Raichle, 2010). Such an arrangement is critical for generating the ubiquitous oscillations of the cortex recorded by EEG and fMRI but its contribution (and other subcortical components) to regulating the DMN in health and disease is largely unexplored. On this basis, we chose to investigate the impact of impaired thalamo-cortical microscopic white matter anatomy on interactions in the DMN in aMCI patients.

We performed constrained spherical deconvolution (CSD)-based probabilistic fibre tractography of the thalamo-DMN white matter pathways in a cohort of older adults with aMCI and healthy age-matched controls (HCs). We also examined the effective connectivity of the resting state thalamo-DMN interactions using a spatio-temporal formulation of Granger Causality (GC). In contrast to simple statistical correlation (i.e. functional connectivity), effective connectivity is more ambitious and attempts to quantify the causal influence one region exerts over another. Given that thalamo-cortical neural signals appear to coordinate distributed networks (Di & Biswal, 2014), such an approach provides greater scope for clarifying the interactions between thalamus and cortex during the transition between health and disease. We predicted that abnormal DMN causal activity would be linked to structural deficits in the thalamo-DMN pathway.

2. Methods

2.1. Participants

Twenty six HC participants and 20 older participants with aMCI took part in the study. The HCs were community-dwelling older adults recruited from the greater Dublin area (Ireland) via newspaper advertisements. They underwent a health screening questionnaire and a neuropsychological assessment, the Consortium to Establish a Registry for Alzheimer's Disease (CERAD; Morris et al., 1989), in order to rule out possible cognitive impairment before inclusion in the study. The CERAD battery has been shown to be sensitive to the presence of age related cognitive decline (Welsh, Butters, Hughes, Mohs, & Heyman, 1991; Welsh, Butters, Hughes, Mohs, & Heyman, 1992). All of the older participants included in

the study scored no more than 1.5 SD below the standardized mean scores for subjects of a similar age and education level on any of the sub-tests. The aMCI participants were recruited from memory clinics in St. James Hospital and St. Patrick's Hospital in Dublin, Ireland, and were diagnosed by a clinician according to the Peterson criteria (Petersen et al., 1999) – i.e., abnormal memory scores for age and education level with no dementia. Four were single amnestic aMCI, and 16 were multi-domain aMCI (Petersen, 2004). Neuropsychological measures were administered or supervised by an experienced neuropsychologist and included the mini-mental state examination (MMSE; Folstein et al., 1975) and Cambridge cognitive examination (Huppert, Brayne, Gill, Paykel, & Beardsall, 1995).

All of the participants were right-handed with no history of head trauma, neurological disease, stroke, transient ischemic attack, heart attack, or psychiatric illness. They completed the Geriatric Depression Scale (GSD; Yesavage et al., 1983), the Eysenck Personality Questionnaire Revised Edition Short Scale (EPQ-R; Eysenck and Eysenck, 1994), and a Cognitive Reserve Questionnaire (Rami et al., 2011) before the MRI scan (table 1). The groups did not differ in terms of age, gender, education level, or levels of cognitive reserve as assessed by the self-report Cognitive Reserve Questionnaire. The aMCI group had lower MMSE scores, higher GDS scores, and scored lower on the EPQ measure of extraversion than the HC group. The study had full ethical approval from the St. James Hospital and the Adelaide and Meath Hospital, incorporating the National Children's Hospital Research Ethics Committee and St Patrick's University Hospital Research Ethics Committee. All participants gave written informed consent before taking part in the study.

2.2. MRI data acquisition

Whole-brain high angular resolution diffusion imaging (HARDI) data were acquired on a 3.0 Tesla Philips Intera MR system (Best, The Netherlands) equipped with an eight channel head coil. A parallel sensitivity encoding (SENSE) approach (Pruessmann, Weiger, Scheidegger, & Boesiger, 1999) with a reduction factor of two was used during the diffusion weighted image (DWI) acquisition. Single-shot spin echo-planar imaging was used to acquire the DWI data with the following parameters: Echo time (TE) 79ms, repetition time (TR) 20,000ms, field of view (FOV) 248mm, matrix 112×112, isotropic voxel of 2.3mm×2.3mm×2.3mm, and 65 slices with 2.3mm thickness with no gap between the slices. Diffusion gradients were applied in 61 isotropically distributed orientations with b =3000s/mm^2, and four images with b=0s/mm^2 were also acquired. A high-resolution 3D T1-weighted anatomical image was acquired for each participant with the following parameters: TE=3.9ms, TR=8.5ms, FOV=230mm, slice thickness=0.9mm, voxel size=0.9mm×0.9mm×0.9mm. ~~These images were used for the correction of EPI-induced geometrical distortions in the DWI data.~~ Resting-state fMRI data were also acquired during the scanning session. The scan lasted for 7 minutes during which time the participants were asked to keep their eyes open and fixate on a cross hairs in the centre of a screen behind the MR scanner, visible via a mirror. The BOLD signal changes were measured using a T2*-weighted echo-planar imaging sequence with TE=30ms and TR=2000ms. Each volume of data covered the entire brain with 39 slices, and the slices were acquired in interleaved sequence from inferior to superior direction. Two hundred ten volumes of data were acquired, with voxel dimensions of 3.5mm×3.5mm×3.85mm and a 0.35mm gap between the slices.

2.3. Face-name encoding and recognition task protocol

Relationships between the participants structural/effective connectivity measures and memory were subsequently examined using data obtained from a face–name recognition task following the resting-state scan. The participants viewed a series of 27 emotional faces (Erwin et al., 1992) with a name presented underneath each one. This task was an implicit

memory task, in that the participants later completed a surprise memory tasks to test their retention of both the faces and the face–name pairs, however, at the time of encoding, they were not explicitly asked to remember the face–name pairs. Rather, the participants were instructed to judge whether the names matched or suited the faces. It was explained that this was a subjective decision, with no right or wrong answer. The participants responded yes or no by pressing a button on a MR-compatible response pad held in their right or left hand, respectively, using the index finger of either hand. Each face–name combination was presented for 4 sec and was shown twice during the run. The faces were positive, negative, or neutral in valence and there were equal numbers of valence types as well as gender. The presentation of the face–name pairs was grouped according to the emotional valence of the faces. In each instance, a group of either two, three, or four faces of one valence type was presented randomly using an event-related paradigm, subsequently, there was a delay during which a white cross hair was presented (control condition). The duration of the white cross was varied according to the duration of the face stimulus. For instance, if a single face was presented for 4 sec the subsequent white cross was also shown for 4 sec and then the next block of faces began. The stimuli were delivered using Presentation v.16.1 (Neurobehavioral Systems, Albany, CA).

Approximately 15 min following the encoding phase, the participants performed a short computer-based recognition task. The emotional faces were presented one at a time on a black background with three names underneath. One of the names was the correct name; one name was a name that had been paired with a different face (distractor; incorrect name), while the third name was a new name (foil; incorrect name). The participants responded by pressing a button on the left, middle, or right side of a keyboard to correspond with the relative position of the name on the screen. The stimuli were presented for 5 sec and followed by an inter-trial interval of 5 sec. This longer trial length was to facilitate performance of this task as it was quite challenging. Before the task began, the participants completed a short practice run of five trials.

2.4. Resting state pre-processing

FMRI data processing was carried out using FEAT (FMRI Expert Analysis Tool) Version 6.00, part of FMRIB's Software Library (FSL; www.fmrib.ox.ac.uk/fsl). Registration to high resolution structural and/or standard space images was carried out using FNIRT (Andersson, Jenkinson, & Smith, 2007). The following pre-statistics processing was applied; motion correction using MCFLIRT (Jenkinson, Bannister, Brady, & Smith, 2002), slice-timing correction using Fourier-space time-series phase-shifting, non-brain removal using BET (Smith, 2002), spatial smoothing using a Gaussian kernel of FWHM 3.0mm, grand-mean intensity normalisation of the entire 4D dataset by a single multiplicative factor, highpass temporal filtering (Gaussian-weighted least-squares straight line fitting, with sigma=50.0s).

2.5. Resting state effective connectivity

GC is a standard statistical tool for detecting the directional influence one system component exerts over another. The concept, originally introduced by Wiener, (1956), and later incorporated into a data analysis framework by Granger, (1969) is described as follows. If historical information from time series X significantly improves prediction accuracy of the future of time series Y in a multivariate autoregressive model (MVAR), GC is identified. This may be viewed of as a measure of model prediction error where GC quantifies the reduction in prediction error when past values of X are included in the explanatory variables of Y (Schelter, Winterhalder, & Timmer, 2006). By fitting a time invariant MVAR model to the experimental time series the classic GC formulation ignores crucial time-varying properties of the system. Such an approach makes the tacit assumption that the longer the time series,

the more reliable the GC estimates. While this may be correct in static circuit representations (Smith et al., 2011), under time-varying conditions this principle is no longer valid. A more robust method is to divide the time series into equal windows and consider them separately. Here, an optimal trade-off between the length of the time windows and the accuracy of the estimated coefficients for each window must be determined. Time windows that are too short prevent the accurate estimation of parameters, while time windows that are too long increase the probability of incorrect inferences of GC. Accordingly, the current paper utilises a novel spatio-temporal GC formulation to quantify the effective connectivity changes between region of interest (ROI; Luo et al., 2013). In this framework, finding the optimal time window length reduces to the solution of a constrained optimisation problem,

$$min_{l_0(m)}\left(GC_{err}\left(l_0(m)\right)+\frac{1}{GC_{avg}\left(l_0(m)\right)}\right)$$

where we seek to simultaneously minimise model prediction error GC_{err} (i.e. the weighted average of the variances of the residuals in each time window) and maximise detected causality information GC_{avg} (i.e. the average GC over all time windows) . This is performed for time windows of different length $l_0(m)=\{t_1,\ldots,t_m\}$. The time window producing the lowest Bayesian information criterion (BIC) is considered optimal. By considering optimal time windows, the spatio-temporal framework allows a more reliable and precise estimate of GC in experimental datasets with time varying properties. This approach has been shown to yield more accurate estimates of GC on resting state fMRI data than traditional GC metrics. In this case, the last 208 time points for each region under consideration were extracted from the functional image volume and divided into four windows with the first two time points removed to avoid start up transients. In terms of spatial resolution, GC is calculated between all pairs of voxels from the two ROI under consideration. The mean GC among all pairs of voxels was then used as the final estimate.

2.6. CSD white matter tractography using MRtrix3

A method for controlling free water contamination of tissue and the resultant partial volume effects is especially important around the fornix where atrophy and cerebrospinal fluid (CSF) is prevalent. The free water elimination technique (Pasternak, Sochen, Gur, Intrator, & Assaf, 2009) has been successfully applied in previous tractography studies of ageing and aMCI (C Metzler-Baddeley et al., 2012; Claudia Metzler-Baddeley, Hunt, et al., 2012; Fletcher, Carmichael, Pasternak, Maier-Hein, & DeCarli, 2014; Kehoe et al., 2015) however at higher b-values the Gaussian assumption underlying the bi-tensor model is no longer valid and a more simple heuristic is indicated. Accordingly, we use the standard free water elimination approach to identify and mask voxels with high free water content but fit the conventional DTI model to each voxel.

The *dwipreproc* preprocessing script was to perform eddy current-induced distortion and motion correction using the FSL tool eddy (Andersson & Sotiropoulos, 2016). The standard MRtrix3 processing script *dwibiascorrect* was used to eliminate low frequency intensity inhomogeneities across the DWI series. The script uses bias field correction algorithms available in the FSL software package (Y. Zhang, Brady, & Smith, 2001).

Probabilistic white matter tractography was performed on the DWIs using the MRtrix3 software package (http://www.mrtrix.org/). Crossing fibres were resolved using the constrained spherical deconvolution algorithm (Tournier, Calamante, Gadian, & Connelly, 2004; Tournier, Calamante, & Connelly, 2012). MRtrix3 pre-processing included computing the diffusion tensors images (or diffusion ellipsoids) for each voxel from which the fractional

anisotropy (FA), axial (DA), radial (RD) and mean (MD) diffusivity images were subsequently generated.

Whole-brain tractography was performed using every voxel as a seed point. The principle diffusion orientation at each point was estimated by the CSD tractography algorithm, which propagated in 0.1 mm steps along this direction. At each new location the fibre orientation(s) was estimated before the tracking moved a further 0.1 mm along the direction that subtended the smallest angle to the current trajectory. A trajectory was followed through the data until the scaled height of the fibre orientation density function peak dropped below the default threshold, or the direction of the pathway changed through an angle of more than 90°.

Anatomical masks were used to divide the results into circumscribed regions. The DMN was defined by probabilistic template (Wang et al., 2014) and the hippocampus and thalamus using the Harvard-Oxford subcortical structural atlas (Fig. 1). Streamlines beginning in one mask and terminating in another were considered in a pairwise fashion for all region of interest. In addition, the FSL tool FAST (FMRIB's Automated Segmentation Tool) was used to derive a white matter brain mask to constrain tractography. Any tracks tracts exiting the white matter were considered spurious and discarded. Tracts were prevented from propagating between hemispheres by a stop region placed down the midline corresponding to the corpus callosum.

Statistically significant differences in the mean FA, DA, RD and MD of tracks in HC versus aMCI were tested by way of a two tailed two sample t-test at $p < 0.05$ corrected for multiple comparisons.

2.7. Independent component analysis (ICA)

The DMN was identified for each subject using ICA. Analysis was carried out using Probabilistic ICA (Beckmann & Smith, 2004) as implemented in MELODIC (Multivariate Exploratory Linear Decomposition into Independent Components) Version 3.14, part of FSL. The following data pre-processing was applied to the input data: masking of non-brain voxels, voxel-wise de-meaning of the data, normalisation of the voxel-wise variance. Pre-processed data were whitened and projected into a 62-dimensional subspace using probabilistic Principal Component Analysis where the number of dimensions was estimated using the Laplace approximation to the Bayesian evidence of the model order (Minka, 2001; Beckmann & Smith, 2004). The whitened observations were decomposed into sets of vectors which describe signal variation across the temporal domain (time-courses) and across the spatial domain (maps) by optimising for non-Gaussian spatial source distributions using a fixed-point iteration technique (Hyvärinen, 1999). Estimated component maps were divided by the standard deviation of the residual noise and thresholded by fitting a mixture model to the histogram of intensity values (Beckmann & Smith, 2004). The number of components was automatically estimated. The component corresponding to the DMN was selected by cross correlating all the components with a probabilistic DMN template (Wang et al., 2014). The fMRI BOLD signal was extracted from DMN components mPFC, MTG, IPL, and PCC, combined with those extracted from hippocampus and thalamus masks, and analysed using the spatio-temporal GC method to determine the effective connectivity. A standard two tailed t-test was used to determine significant differences between the HC and aMCI patients at $p < 0.05$ corrected for multiple comparisons.

3. Results

3.1. Comparison of resting state thalamo-DMN effective connectivity in HC versus aMCI subjects

The spatio-temporal GC effective connectivity analysis revealed significant differences in a circumscribed set of regions at the Bonferroni corrected threshold of $p < 0.0014$.

In aMCI, several incoming connections to PCC and left IPL showed reduced casual connectivity. An especially pronounced decrease in causal interaction to left IPL from other DMN components, hippocampus, and thalamus was observed (Fig. 2A). Reduced connectivity to left IPL included incoming connections from left thalamus [$t(44) = 3.77$, $p < 0.001$], left [$t(44) = 4.3$, $p < 0.0001$] and right [$t(44) = 3.80$, $p < 0.001$] MTG and from right IPL [$t(44) = 3.83$ $p < 0.001$]. These changes correspond to a highly significant [$t(44) = 5.10$, $p < 0.00001$] decrease in average FA in the white matter between left thalamus and left IPL (Fig. 2B).

Also in aMCI, significant reductions in connectivity to PCC from left MTG [$t(44) = 3.93$, $p < 0.001$] were found, together with significant reductions in connectivity to right IPL from PCC [$t(44) = 3.73$, $p < 0.001$] (Fig. 2A).

3.2. Comparison of thalamo-DMN microstructural integrity in HC versus aMCI subjects

In aMCI, CSD white matter tractography identified statistically significant increases at the Bonferroni corrected threshold in average DA, RD, and MD in the white matter fibre pathways connecting thalamus to hippocampus, PCC, and IPL (Fig. 3). Significant decreases in average FA were also detected in the white matter between thalamus and IPL. These included:

Significant decreases in FA (Fig. 2B) between right thalamus and right IPL [$t(44) = 3.81$, $p < 0.001$] and between left thalamus and left IPL [$t(44) = 5.24$, $p < 0.00001$].

Significant increases in DA (Fig. 2C) between right thalamus and right hippocampus [$t(44) = -4.68$, $p < 0.0001$], right hippocampus and PCC [$t(44) = -4.02$, $p < 0.001$], left thalamus and left hippocampus [$t(44) = -5.33$, $p < 0.00001$], left thalamus and PCC [$t(44) = -3.91$, $p < 0.001$], left hippocampus and left IPL [$t(44) = -4.13$ $p < 0.001$], and left hippocampus and PCC [$t(44) = -3.91$, $p < 0.001$].

These changes were recapitulated in the MD metric (Fig. 2D) with significant increases between right hippocampus and PCC [$t(44) = -3.69$, $p < 0.001$], left thalamus and left hippocampus [$t(44) = -4.34$, $p < 0.0001$], left thalamus and PCC [$t(44) < -3.63$, $p = 0.001$] and left hippocampus and PCC [$t(44) = -4.17$, $p < 0.001$].

Finally, a significant increase in RD (Fig. 2E) between left hippocampus and PCC [$t(44) = -3.66$, $p < 0.001$] was also found.

3.3. Empirical measures of effective and structural connectivity predict memory performance

To investigate whether empirical measures of effective and structural connectivity relate to memory, we regressed the diffusivity and GC metrics against the results from a face-name encoding and recognition task using gender, age, and motion parameter estimates as covariates of no interest.

The aMCI cohort displayed a significant negative correlation between the integrity of the left thalamo-cortical white matter connectivity and memory in three DMN regions (Fig. 4A) including IPL [$t(24) = -2.43$, $p < 0.05$], hippocampus [$t(24) = -2.31$, $p < 0.05$], and PCC [$t(24) = -2.21$, $p < 0.05$]. The healthy subjects displayed no such relationship.

Conversely, the healthy cohort demonstrated a significant negative correlation between the effective connectivity of IPL and memory and three other DMN regions (Fig. 4B) including left MTG [$t(24) = -2.47$, $p < 0.05$], right IPL [$t(24) = -2.54$, $p < 0.05$], and PCC [$t(24) = -2.21$, $p < 0.05$]. The same relationship was absent in the aMCI cohort. All results survived multiple-comparison correction with FDR ($q < 0.1$).

4. Discussion

The appearance of atrophy, tangles, and plaques in thalamus is often characterised as a secondary process resulting from atrophy in the hippocampus and the prion-like transmission of pathology along the white matter topography (Raj et al., 2012). But such a view is inconsistent with evidence suggesting that the earliest metabolic changes occur not in hippocampus but in posterior DMN node PCC. Thus, structural deficits in thalamus may be driving early PCC hypometabolism and initiating the cascade of DMN functional anomalies typically associated with early AD. Accordingly, we used a multimodal approach to assess the impact of thalamo-cortico-thalamic feedback loop integrity on DMN functionality in aMCI.

We found significant structural abnormalities in the thalamo-PCC and thalamo-IPL white matter fibre pathways in the aMCI cohort (Fig. 2B, C, D, E). A pronounced reduction in left thalamo-IPL effective connectivity (Fig. 2A) corresponded with significant thalamo-IPL structural impairment (Fig. 2B). Critically, the integrity of thalamic white matter and memory was correlated in the aMCI cohort but not in the HCs (Fig. 4A). In general, the gradient of structural impairment followed a hippocampo-thalamo-PCC axis consistent with a prion-like dissemination of pathology (Raj et al., 2012) along the major white matter fibre pathways of the Papez circuit ((Papez, 1937)). No structural abnormalities were identified between cortical DMN components MPFC, MTG, IPL, and PCC, however significant disruption to incoming IPL effective connectivity was observed, and this distinguished aMCI from HC memory performance (Fig. 4B).

Overall, our findings are broadly suggestive. One interpretation is that disrupted effective connectivity in posterior DMN nodes PCC and IPL is, to some extent, inspired by incipient thalamo-cortical deafferentation. If true, this finding may help explain abnormal task-induced DMN response patterns typically found in aMCI and AD subjects (Pihlajamäki & Sperling, 2009).

4.1. Impaired hippocampo-thalamo-PCC white matter anatomy and abnormal PCC effective connectivity

The current paper identified significant structural impairment between fibre pathways connecting hippocampus and thalamus (Fig. 2C, D), thalamus and PCC (Fig. 2C, D), and PCC and hippocampus (Fig. 2C, D, E). Measures of left thalamo-cortical structural integrity (including tracts to hippocampus and PCC) correlated with memory performance in the aMCI cohort but not in the HCs (Fig. 4A).

Impaired structural relations within the hippocampo-thalamo-PCC complex are likely mediated by their close anatomical association. Together these structures comprise a limbic-diencephalic memory network (Nestor, Fryer, Smielewski, & Hodges, 2003) connected through the circuit of Papez ((Papez, 1937)). This structure runs from hippocampus through fornix to anterior thalamus via mammillary bodies and onto PCC before returning to hippocampus to complete the circuit. Interestingly, the current study identified a decreasing gradient of structural impairment between hippocampus, thalamus, and PCC, suggesting that structural deafferentation of PCC through impaired hippocampus and thalamus fibre pathways, likely stems from pathology and atrophy originating in the hippocampal complex.

Such a view is consistent with postmortem studies indicating that thalamic nuclei connected to hippocampus are a site of primary degeneration in AD (Xuereb et al., 1991).

Previous work has highlighted a staged disconnection process occurring both along the cingulum bundle between hippocampus and PCC (i.e. the direct route) and within the memory circuit of Papez encompassing thalamic intermediaries (i.e. the indirect route; Villain et al., 2008). Such findings are consistent with early PCC hypometabolism (Matsuda, 2001; Valla, Berndt, & Gonzalez-Lima, 2001; Mosconi et al., 2008; Zhu, Majumdar, Korolev, Berger, & Bozoki, 2013; Mutlu et al., 2016) where it frequently presents before clinical diagnosis (Minoshima et al., 1997; Johnson et al., 1998) as part of a constellation of metabolic effects focused around medial temporal lobe and thalamus, when memory loss is still a relatively isolated feature (Nestor et al., 2003). Interestingly, PCC hypometabolism appears to correlate with remote hippocampus atrophy early in MCI but transition to both remote and local effects over the course of progression to AD (Teipel & Grothe, 2016).

The current study identified a significant correlation between the structural integrity of hippocampo-thalamus and thalamo-PCC fibre pathways (i.e. the indirect route) and memory in the aMCI cohort which was absent in the HCs (Fig. 4A). A similar pattern was identified in the hippocampo-PCC fibre pathway (i.e. the direct route) however this did not survive correction for multiple comparisons. Dysfunction of structures along the hippocampal output pathways to PCC have been linked to episodic memory impairment (Yakushev et al., 2011).

The PCC's hub status (Hagmann et al., 2008) may predispose to amyloid deposition, atrophy, and hypometabolism (Buckner et al., 2005, 2009) where remote often diffuse damage accumulates as altered PCC connectivity through a form of diaschisis (Meguro et al., 1999; Leech & Sharp, 2014). One suggestion is that direct thalamo-PCC (Fig. 2C, D) and distal thalamo-IPL (Fig. 2B) white matter structural deficits operate in tandem to initiate a cascade of aberrant effective connectivity in PCC (Fig. 2A). Taken together, these findings are consistent with a progressive disconnection of PCC from downstream cortical and subcortical sources with differential effects operating on the direct versus indirect hippocampo-PCC pathways.

4.2. Impaired thalamo-IPL white matter anatomy and abnormal IPL effective connectivity

The current paper identified significant impairments in thalamic white matter circuitry serving bilateral IPL where the magnitude of diffusivity change (Fig. 2B) correlated with the intensity and extent of effective connectivity disruption in each hemisphere (Fig 2A).

Marked structural deficits were observed in left thalamo-IPL white matter connectivity together with significantly reduced effective connectivity from left thalamus. In the aMCI cohort, measures of reduced thalamo-IPL structural integrity correlated with memory performance (Fig. 4A). Left thalamo-IPL structural abnormalities were accompanied by widespread decreases in effective connectivity from other DMN regions. Similarly, in right hemisphere, thalamo-IPL structural deficits coocurred with disrupted incoming and outgoing IPL effective connectivity. Crucially, the relationship between IPL effective connectivity and memory was disrupted in the aMCI subjects but not in the HCs (Fig. 4B).

Several converging findings implicate the pulvinar nucleus of the thalamus in this dysfunction. The pulvinar nuclei appear to play a role in cortico-cortical communication where they receive driving input from IPL and relay signals back to cortex via ascending thalamo-cortical projections (Saalmann, Pinsk, Wang, Li, & Kastner, 2012). Since direct cortico-cortical projections far outnumber projections to pulvinar nucleus from cortex, the pulvinar is unlikely to be the primary route for the transfer of cortico-cortical sensory signals,

rather, it may act to coordinate interactions between distributed cortical networks as a function of attention (Basso, Uhlrich, & Bickford, 2005). Interestingly, entorhinal cortex connects directly to pulvinar nucleus via a non-fornical temporopulvinar tract (Saunders, Mishkin, & Aggleton, 2005; Zarei et al., 2013) which may provide a conduit for the prion-like transsynaptic spread of disease agents originating in hippocampus (Raj et al., 2012). Consistent with this hypothesis, the present study identified significant structural impairment between thalamus and hippocampus (Fig. 2C, D).

Taken together, these findings are consistent with the idea that disrupted posterior DMN node effective connectivity is, to some extent, mediated by impaired thalamo-cortical white matter circuitry.

4.3. Methodological considerations

Some limitations should be noted. The major weakness of the paper is that each thalamic nucleus has specific cortical connections and functions, yet the present analysis uses a holo-thalamic approach. It would be more informative to determine whether sub-nuclei show differential causal interactions between specific regions of thalamus and crucial DMN nodes and likewise, whether these connections show varying degrees of structural impairment. Such an approach would reveal the specificity of AD pathology for individual thalamic nuclei. Analysing the entire thalamus may dilute these results. Our findings should therefore be considered as preliminary evidence warranting further investigation.

It should also be noted that the indirect relationship between fMRI BOLD signal and the underlying neural mechanism is especially problematic when applying GC and should be noted as a weakness in the present study. Firstly, the study's sampling rate (repetition time or TR) of two seconds is considerably slower than the millisecond temporal resolution of the neuronal activity we seek to qualify. Secondly, the temporal precedence assumptions of GC can be violated by regional differences in the latency of the hemodynamic response (Handwerker, Ollinger, & D'Esposito, 2004; Friston, 2011). Since neurovascular coupling can be altered in complex ways by disease, the likelihood of such an event is magnified in the aMCI patient cohort (Handwerker, Gonzalez-Castillo, D'Esposito, & Bandettini, 2012). One typical scenario, is that region X causally influences Y at the neuronal level but has a longer time-to-peak in its HRF due to pathology of the neurovasculature. Thus, GC analysis of BOLD signal may incorrectly suggest that Y is causally implicated in causing X. Simulations show that GC performs well when the HRF delay between regions is short (Deshpande, Sathian, & Hu, 2010; Schippers, Renken, & Keysers, 2011) however sufficiently fast sampling, on par with the neuronal delays themselves, is required to ensure GC is fully invariant to HRF latency (Seth, Chorley, & Barnett, 2013). Other simulations suggest that the relationship between GC at the neuronal level and GC at the fMRI level is reasonably preserved over a range of sampling rates and convolution parameters (Wen, Rangarajan, & Ding, 2013). Whatever the case, sub-second temporal resolutions have been made available (Feinberg et al., 2010; Feinberg & Yacoub, 2012) and are standard as part of the Human Connectome Project (Van Essen et al., 2013). The most recent advances enable a temporal resolution as fast as 50 ms (Boyacioğlu & Barth, 2013).

Critically, GC makes no claims regarding the underlying physical mechanisms responsible for the observed differences in causal relationships between regions. In contrast, the dynamic causal modelling approach (DCM; Di & Biswal, 2014b) explicitly specifies dynamic effective relationships at the neuronal level, allowing the most likely structural model for generating the observed data to be identified. Applying DCM in future studies will help clarify thalamic involvement in posterior DMN dysfunction.

The choice of CSD-based tractography reflects the growing recognition that assumptions underlying the DTI model may not always be met in practice (Wheeler-Kingshott & Cercignani, 2009; Jones, 2010; Jones & Cercignani, 2010). The DTI model can only capture a unitary fibre direction within a single voxel despite observations that ninety percent of the brain is composed of multiple crossing fibres (Jeurissen, Leemans, Tournier, Jones, & Sijbers, 2013). For this reason CSD attempts to map several fibre directions per voxel by taking advantage of the high number of diffusion encoding directions and large b-values acquired using the HARDI acquisition protocol (Tournier, Calamante, & Connelly, 2007; Tournier et al., 2008; Mielke et al., 2012; Farquharson et al., 2013). Using large b-values has an additional advantage. By allowing a sufficiently long diffusion path to be measured water molecules are more likely to collide with their container. This may be relevant in patients with neurodegenerative disorders who have increased permeability of membranes, greater extracellular space due to axonal atrophy, demyelination and glial pathology (Acosta-Cabronero & Nestor, 2014). To date, only a handful of tractography studies have utilised HARDI data and large b-values (de Schotten et al., 2011; Meng et al., 2013; Yeatman et al., 2014; Xie et al., 2015) and only one specifically in clinical aMCI and AD (Kehoe et al., 2015).

The absence of indirect biomarkers of AD pathology (CSF biomarkers and/or amyloid PET imaging) should also be acknowledged as a weakness in the present paper.

4.4. Conclusion

The dynamic nature of thalamo-cortical dialogue suggests that abnormalities in DMN operation may best be understood from the perspective of thalamic dysfunction. The present study employed diffusion imaging and effective connectivity to clarify the relationship between the physical integrity of thalamic white matter projections and the activity of the DMN. Significant changes in the diffusivity metrics of thalamic white matter projection tracts to hippocampus, PCC and IPL (Fig. 2B, C, D) were identified. Effective connectivity changes corresponding to the same regions were also observed (Fig. 2A). Interestingly, no structural deficits were found between DMN nodes suggesting that early changes in DMN activity ~~are~~ could be a result of impaired thalamo-cortical structural integrity.

Such a conclusion is supported by previous resting state MEG (Garcés et al., 2014), EEG (Schreckenberger et al., 2004; Garcés et al., 2013; Moretti, 2015), and fMRI (Greicius, Srivastava, Reiss, & Menon, 2004; Sorg et al., 2007; Damoiseaux, Prater, Miller, & Greicius, 2012) studies citing disruption in posterior thalamo-cortical alpha sources. Significant evidence suggests that thalamo-cortical circuitry underlie the generation and modulation of alpha and theta rhythms and that average power is attenuated in these frequency bands for MCI and AD subjects (Jeong, 2004; Koenig et al., 2005; Jelles et al., 2008; Park et al., 2008). Several recent modelling studies have proposed a candidate mechanism citing impairment to thalamic reticular fibres in MCI and AD as the source of the dysfunction (Bhattacharya, Coyle, & Maguire, 2011; Li, Coyle, Maguire, Watson, & McGinnity, 2011; Bhattacharya, Cakir, Serap-Sengor, Maguire, & Coyle, 2013; Abuhassan, Coyle, & Maguire, 2014).

A corollary of this discussion is the extent to which cortical activity is dependent on cortico-cortical verses thalamo-cortical connections. It has been suggested that thalamic nuclei coordinate distributed cortical regions through cortico-thalamo-cortical pathways. Abnormalities originating in thalamic to PCC and IPL white matter may therefore be sufficient to engender posterior DMN dysfunction without appealing to comparable deficits in cortico-cortical tracts between DMN nodes. Such a view is consistent with the anatomy and timeline of pathogenesis with thalamic nuclei demonstrating pathology an earlier stage of the disease than cortex. Cortical atrophy may therefore be in response to thalamic white

matter disruption with commensurate causal abnormalities occurring in response to changes in thalamo-cortical signalling rather than being instigated by structural changes within the cortex. Importantly, the present study is unable to confirm this hypothesis. Other scenarios, in which cortical pathology is causing a degeneration of thalamo-cortical tracts is also possible or likewise, a parallel disruption in both thalamus and cortex.

Overall, these results provide a compelling and previously unexplored physical basis for posterior DMN dysfunction and abnormal fMRI task-induced deactivation response patterns in aMCI and AD patients and underscore the need to consider neurodegenerative changes within a wider system context including contributions of both cortical and subcortical thalamic components. This work complements a growing body of evidence that suggests effective connectivity is disrupted in neurodegenerative disorders such as aMCI and AD and that these changes are underpinned by structural deficits. For these reasons, joint effective and structural studies will play an increasingly important role in the future as we seek to understand how pathological changes in structural connectivity are reflected in altered network effective connectivity.

Acknowledgements

The research was funded by a Department for Employment and Learning Northern Ireland PhD studentship and the data collection was supported by the Northern Ireland Department for Education and Learning under the Strengthening the All Island Research Base programme. ALWB was funded in part by the Science Foundation Ireland Stokes Programme (07/SK/B1214a). RAK and BL funded in part by the Health Research Board (Ireland).

Bibliography

Abuhassan, K., Coyle, D., & Maguire, L. (2014). Compensating for thalamocortical synaptic loss in Alzheimer's disease. *Frontiers in Computational Neuroscience*, *8*(June), 65. https://doi.org/10.3389/fncom.2014.00065

Acosta-Cabronero, J., & Nestor, P. J. (2014). Diffusion tensor imaging in Alzheimer's disease: insights into the limbic-diencephalic network and methodological considerations. *Frontiers in Aging Neuroscience*, *6*, 266. https://doi.org/10.3389/fnagi.2014.00266

Aggleton, J. P., O'Mara, S. M., Vann, S. D., Wright, N. F., Tsanov, M., Erichsen, J. T., … Erichsen, J. T. (2010). Hippocampal-anterior thalamic pathways for memory: Uncovering a network of direct and indirect actions. *European Journal of Neuroscience*, *31*(12), 2292–2307. https://doi.org/10.1111/j.1460-9568.2010.07251.x

Andersson, J. L. R., Jenkinson, M., & Smith, S. (2007). *Non-linear registration aka Spatial normalisation FMRIB Technial Report TR07JA2*. *In Practice*. Retrieved from http://fmrib.medsci.ox.ac.uk/analysis/techrep/tr07ja2/tr07ja2.pdf

Andersson, J. L. R., & Sotiropoulos, S. N. (2016). An integrated approach to correction for off-resonance effects and subject movement in diffusion MR imaging. *NeuroImage*, *125*, 1063–1078. https://doi.org/10.1016/j.neuroimage.2015.10.019

Basso, M. A., Uhlrich, D., & Bickford, M. E. (2005). Cortical function: a view from the thalamus. *Neuron*, *45*(4), 485–8. Retrieved from http://www.ncbi.nlm.nih.gov/pubmed/15756758

Beckmann, C. F., & Smith, S. M. (2004). Probabilistic Independent Component Analysis for Functional Magnetic Resonance Imaging. *IEEE Transactions on Medical Imaging*, *23*, 137–152. https://doi.org/10.1109/TMI.2003.822821

Bhattacharya, B. Sen, Coyle, D., & Maguire, L. P. (2011). A thalamo-cortico-thalamic neural mass model to study alpha rhythms in Alzheimer's disease. *Neural Networks*, *24*(6), 631–645. https://doi.org/10.1016/j.neunet.2011.02.009

Boyacioğlu, R., & Barth, M. (2013). Generalized inverse imaging (GIN): Ultrafast fMRI with physiological noise correction. *Magnetic Resonance in Medicine*, *70*(4), 962–971. https://doi.org/10.1002/mrm.24528

Braak, H., & Braak, E. (1991a). Alzheimer's disease affects limbic nuclei of the thalamus. *Acta Neuropathologica*, *81*, 261–268. https://doi.org/10.1007/BF00305867

Braak, H., & Braak, E. (1991b). Neuropathological stageing of Alzheimer-related changes. *Acta Neuropathologica*, *82*, 239–259. https://doi.org/10.1007/BF00308809

Braak, H., & Braak, E. (1995). Staging of Alzheimer's disease-related neurofibrillary changes. *Neurobiology of Aging*, *16*(3), 271–278. https://doi.org/10.1016/0197-4580(95)00021-6

Buckner, R. L., Andrews-Hanna, J. R., & Schacter, D. L. (2008). The brain's default network: anatomy, function, and relevance to disease. *Annals of the New York Academy of Sciences*, *1124*, 1–38. https://doi.org/10.1196/annals.1440.011

Buckner, R. L., Sepulcre, J., Talukdar, T., Krienen, F. M., Liu, H., Hedden, T., … Johnson, K. a. (2009). Cortical hubs revealed by intrinsic functional connectivity: mapping, assessment of stability, and relation to Alzheimer's disease. *The Journal of Neuroscience : The Official Journal of the Society for Neuroscience*, *29*(6), 1860–73. https://doi.org/10.1523/JNEUROSCI.5062-08.2009

Buckner, R. L., Snyder, A. Z., Shannon, B. J., LaRossa, G., Sachs, R., Fotenos, A. F., … Mintun, M. a. (2005). Molecular, structural, and functional characterization of Alzheimer's disease: evidence for a relationship between default activity, amyloid, and memory. *The Journal of Neuroscience : The Official Journal of the Society for Neuroscience*, *25*(34), 7709–17. https://doi.org/10.1523/JNEUROSCI.2177-05.2005

Burns, A., & Iliffe, S. (2009). Alzheimer's disease. *BMJ (Clinical Research Ed.)*, *338*, b158. Retrieved from http://www.ncbi.nlm.nih.gov/pubmed/19196745

Cantero, J. L., Atienza, M., Gomez-Herrero, G., Cruz-Vadell, A., Gil-Neciga, E., Rodriguez-Romero, R., & Garcia-Solis, D. (2009). Functional integrity of thalamocortical circuits

differentiates normal aging from mild cognitive impairment. *Human Brain Mapping*, *30*(12), 3944–57. https://doi.org/10.1002/hbm.20819

Cherubini, A., Péran, P., Spoletini, I., Di Paola, M., Di Iulio, F., Hagberg, G. E., … Spalletta, G. (2010). Combined volumetry and DTI in subcortical structures of mild cognitive impairment and Alzheimer's disease patients. *Journal of Alzheimer's Disease : JAD*, *19*, 1273–1282. https://doi.org/10.3233/JAD-2010-091186

Chételat, G., Landeau, B., Eustache, F., Mézenge, F., Viader, F., de la Sayette, V., … Baron, J.-C. (2005). Using voxel-based morphometry to map the structural changes associated with rapid conversion in MCI: a longitudinal MRI study. *NeuroImage*, *27*(4), 934–46. https://doi.org/10.1016/j.neuroimage.2005.05.015

Chhatwal, J. P., Schultz, A. P., Johnson, K., Benzinger, T. L. S., Jack, C., Ances, B. M., … Sperling, R. a. (2013). Impaired default network functional connectivity in autosomal dominant Alzheimer disease. *Neurology*, *81*(8), 736–44. https://doi.org/10.1212/WNL.0b013e3182a1aafe

Chiang, G. C., Zhan, W., Schuff, N., & Weiner, M. W. (2012). White matter alterations in cognitively normal apoE ??2 carriers: Insight into Alzheimer resistance? *American Journal of Neuroradiology*, *33*(7), 1392–1397. https://doi.org/10.3174/ajnr.A2984

Damoiseaux, J. S., Prater, K. E., Miller, B. L., & Greicius, M. D. (2012). Functional connectivity tracks clinical deterioration in Alzheimer's disease. *Neurobiology of Aging*, *33*(4), 828.e19-30. https://doi.org/10.1016/j.neurobiolaging.2011.06.024

Damoiseaux, J. S., Rombouts, S. A. R. B., Barkhof, F., Scheltens, P., Stam, C. J., Smith, S. M., & Beckmann, C. F. (2006). Consistent resting-state networks across healthy subjects. *Proceedings of the National Academy of Sciences of the United States of America*, *103*(37), 13848–53. https://doi.org/10.1073/pnas.0601417103

de Jong, L. W., van der Hiele, K., Veer, I. M., Houwing, J. J., Westendorp, R. G. J., Bollen, E. L. E. M., … van der Grond, J. (2008). Strongly reduced volumes of putamen and thalamus in Alzheimer's disease: an MRI study. *Brain : A Journal of Neurology*, *131*(Pt 12), 3277–85. https://doi.org/10.1093/brain/awn278

de Schotten, M. T., Dell'Acqua, F., Forkel, S. J., Simmons, A., Vergani, F., Murphy, D. G. M., & Catani, M. (2011). A lateralized brain network for visuospatial attention. *Nature Neuroscience*, *14*(10), 1245–1246. https://doi.org/10.1038/nn.2905

Deshpande, G., Sathian, K., & Hu, X. (2010). Effect of hemodynamic variability on Granger causality analysis of fMRI. *NeuroImage*, *52*(3), 884–896. https://doi.org/10.1016/j.neuroimage.2009.11.060

Di, X., & Biswal, B. B. (2014). Modulatory interactions between the default mode network and task positive networks in resting-state. *PeerJ*, *2*, e367. https://doi.org/10.7717/peerj.367

Drzezga, A., Becker, J. A., Van Dijk, K. R. a, Sreenivasan, A., Talukdar, T., Sullivan, C., … Sperling, R. a. (2011). Neuronal dysfunction and disconnection of cortical hubs in non-demented subjects with elevated amyloid burden. *Brain : A Journal of Neurology*, *134*(Pt 6), 1635–46. https://doi.org/10.1093/brain/awr066

Erwin, R. J., Gur, R. C., Gur, R. E., Skolnick, B., Mawhinney-Hee, M., & Smailis, J. (1992). Facial emotion discrimination: I. Task construction and behavioral findings in normal subjects. *Psychiatry Research*, *42*(3), 231–240. https://doi.org/10.1016/0165-1781(92)90115-J

Eysenck, H. J., & Eysenck, S. B. G. (1994). Manual for the Eysenck Personality Questionnaire. *(EPQ-R Adult)*. https://doi.org/10.1177/014662168000400106

Farquharson, S., Tournier, J.-D., Calamante, F., Fabinyi, G., Schneider-Kolsky, M., Jackson, G. D., & Connelly, A. (2013). White matter fiber tractography: why we need to move beyond DTI. *Journal of Neurosurgery*, *118*(June), 1367–77. https://doi.org/10.3171/2013.2.JNS121294

Feinberg, D. A., Moeller, S., Smith, S. M., Auerbach, E., Ramanna, S., Glasser, M. F., … Yacoub, E. (2010). Multiplexed echo planar imaging for sub-second whole brain fmri and fast diffusion imaging. *PLoS ONE*, *5*(12). https://doi.org/10.1371/journal.pone.0015710

Feinberg, D. A., & Yacoub, E. (2012). The rapid development of high speed, resolution and precision in fMRI. *NeuroImage*. https://doi.org/10.1016/j.neuroimage.2012.01.049

Fernández-Espejo, D., Soddu, A., Cruse, D., Palacios, E. M., Junque, C., Vanhaudenhuyse, A., … Owen, A. M. (2012). A role for the default mode network in the bases of disorders of consciousness. *Annals of Neurology*, *72*(3), 335–43. https://doi.org/10.1002/ana.23635

Ferrarini, L., Palm, W. M., Olofsen, H., van der Landen, R., Jan Blauw, G., Westendorp, R. G. J., … Admiraal-Behloul, F. (2008). MMSE scores correlate with local ventricular enlargement in the spectrum from cognitively normal to Alzheimer disease. *NeuroImage*, *39*(4), 1832–8. https://doi.org/10.1016/j.neuroimage.2007.11.003

Fletcher, E., Carmichael, O., Pasternak, O., Maier-Hein, K. H., & DeCarli, C. (2014). Early brain loss in circuits affected by Alzheimer's disease is predicted by fornix microstructure but may be independent of gray matter. *Frontiers in Aging Neuroscience*, *6*(MAY). https://doi.org/10.3389/fnagi.2014.00106

Folstein, M. F., Folstein, S. E., & McHugh, P. R. (1975). "Mini-mental state." *Journal of Psychiatric Research*, *12*(3), 189–198. https://doi.org/10.1016/0022-3956(75)90026-6

Friston, K. J. (2011). Functional and effective connectivity: a review. *Brain Connectivity*, *1*(1), 13–36. https://doi.org/10.1089/brain.2011.0008

Garcés, P., Angel Pineda-Pardo, J., Canuet, L., Aurtenetxe, S., López, M. E., Marcos, A., … Maestú, F. (2014). The Default Mode Network is functionally and structurally disrupted in amnestic mild cognitive impairment - a bimodal MEG-DTI study. *NeuroImage. Clinical*, *6*, 214–21. https://doi.org/10.1016/j.nicl.2014.09.004

Garcés, P., Vicente, R., Wibral, M., Pineda-Pardo, J. Á., López, M. E., Aurtenetxe, S., … Fernández, A. (2013). Brain-wide slowing of spontaneous alpha rhythms in mild cognitive impairment. *Frontiers in Aging Neuroscience*, *5*, 100. https://doi.org/10.3389/fnagi.2013.00100

Granger, C. W. . (1969). Investigating Causal Relations by Econometric Models and Cross-Spectral Methods. *Econometrica*, *37*(3), 424–438. https://doi.org/10.2307/1912791

Greicius, M. D., Krasnow, B., Reiss, A. L., & Menon, V. (2003). Functional connectivity in the resting brain: a network analysis of the default mode hypothesis. *Proceedings of the National Academy of Sciences of the United States of America*, *100*(1), 253–258. https://doi.org/10.1073/pnas.0135058100

Greicius, M. D., Srivastava, G., Reiss, A. L., & Menon, V. (2004). Default-mode network activity distinguishes Alzheimer's disease from healthy aging: evidence from functional MRI. *Proceedings of the National Academy of Sciences of the United States of America*, *101*(13), 4637–42. https://doi.org/10.1073/pnas.0308627101

Hagmann, P., Cammoun, L., Gigandet, X., Meuli, R., Honey, C. J., Wedeen, V. J., & Sporns, O. (2008). Mapping the structural core of human cerebral cortex. *PLoS Biology*, *6*(7), e159. https://doi.org/10.1371/journal.pbio.0060159

Handwerker, D. A., Gonzalez-Castillo, J., D'Esposito, M., & Bandettini, P. A. (2012). The continuing challenge of understanding and modeling hemodynamic variation in fMRI. *NeuroImage*. https://doi.org/10.1016/j.neuroimage.2012.02.015

Handwerker, D. A., Ollinger, J. M., & D'Esposito, M. (2004). Variation of BOLD hemodynamic responses across subjects and brain regions and their effects on statistical analyses. *NeuroImage*, *21*(4), 1639–1651. https://doi.org/10.1016/j.neuroimage.2003.11.029

Hedden, T., Van Dijk, K. R. A., Becker, J. A., Mehta, A., Sperling, R. A., Johnson, K. A., & Buckner, R. L. (2009). Disruption of functional connectivity in clinically normal older adults harboring amyloid burden. *The Journal of Neuroscience : The Official Journal of the Society for Neuroscience*, *29*(40), 12686–94. https://doi.org/10.1523/JNEUROSCI.3189-09.2009

Huppert, F. A., Brayne, C., Gill, C., Paykel, E. S., & Beardsall, L. (1995). CAMCOG--a concise neuropsychological test to assist dementia diagnosis: socio-demographic determinants in an elderly population sample. *The British Journal of Clinical Psychology / the British Psychological Society*, *34 (Pt 4)*, 529–41. Retrieved from http://www.ncbi.nlm.nih.gov/pubmed/8563660

Hyvärinen, A. (1999). Fast and robust fixed-point algorithms for independent component analysis. *IEEE Transactions on Neural Networks*, *10*, 626–634. https://doi.org/10.1109/72.761722

Jelles, B., Scheltens, P., van der Flier, W. M., Jonkman, E. J., da Silva, F. H. L., & Stam, C. J. (2008). Global dynamical analysis of the EEG in Alzheimer's disease: frequency-specific changes of functional interactions. *Clinical Neurophysiology : Official Journal of the International Federation of Clinical Neurophysiology*, *119*(4), 837–41. https://doi.org/10.1016/j.clinph.2007.12.002

Jenkinson, M., Bannister, P., Brady, M., & Smith, S. (2002). Improved optimization for the robust and accurate linear registration and motion correction of brain images. *NeuroImage*, *17*, 825–841. https://doi.org/10.1016/S1053-8119(02)91132-8

Jeong, J. (2004). EEG dynamics in patients with Alzheimer's disease. *Clinical Neurophysiology : Official Journal of the International Federation of Clinical Neurophysiology*, *115*(7), 1490–505. https://doi.org/10.1016/j.clinph.2004.01.001

Jeurissen, B., Leemans, A., Tournier, J.-D., Jones, D. K., & Sijbers, J. (2013). Investigating the prevalence of complex fiber configurations in white matter tissue with diffusion magnetic resonance imaging. *Human Brain Mapping*, *34*(11), 2747–66. https://doi.org/10.1002/hbm.22099

Johnson, K. A., Jones, K., Holman, B. L., Becker, J. A., Spiers, P. A., Satlin, A., & Albert, M. S. (1998). Preclinical prediction of Alzheimer's disease using SPECT. *Neurology*, *50*, 1563–1571. https://doi.org/10.1212/WNL.50.6.1563

Jones, D. K. (2010). Challenges and limitations of quantifying brain connectivity in vivo with diffusion MRI. *Imaging in Medicine*, *2*(3), 341–355. https://doi.org/10.2217/iim.10.21

Jones, D. K., & Cercignani, M. (2010). Twenty-five pitfalls in the analysis of diffusion MRI data. *NMR in Biomedicine*. https://doi.org/10.1002/nbm.1543

Jones, D. T., Mateen, F. J., Lucchinetti, C. F., Jack, C. R., & Welker, K. M. (2011). Default mode network disruption secondary to a lesion in the anterior thalamus. *Archives of Neurology*, *68*(2), 242–247. https://doi.org/10.1001/archneurol.2010.259

Kehoe, E. G., Farrell, D., Metzler-Baddeley, C., Lawlor, B. A., Kenny, R. A., Lyons, D., … Bokde, A. L. (2015). Fornix white matter is correlated with resting-state functional connectivity of the thalamus and hippocampus in healthy aging but not in mild cognitive impairment - A preliminary study. *Frontiers in Aging Neuroscience*, *7*(FEB), 10. https://doi.org/10.3389/fnagi.2015.00010

Knight, W. D., Okello, A. A., Ryan, N. S., Turkheimer, F. E., Rodríguez Martinez De Llano, S., Edison, P., … Rossor, M. N. (2011). Carbon-11-Pittsburgh compound B positron emission tomography imaging of amyloid deposition in presenilin 1 mutation carriers. *Brain*, *134*, 293–300. https://doi.org/10.1093/brain/awq310

Koenig, T., Prichep, L., Dierks, T., Hubl, D., Wahlund, L. O., John, E. R., & Jelic, V. (2005). Decreased EEG synchronization in Alzheimer's disease and mild cognitive impairment. *Neurobiology of Aging*, *26*(2), 165–71. https://doi.org/10.1016/j.neurobiolaging.2004.03.008

Leech, R., & Sharp, D. J. (2014). The role of the posterior cingulate cortex in cognition and disease. *Brain : A Journal of Neurology*, *137*(Pt 1), 12–32. https://doi.org/10.1093/brain/awt162

Li, X., Coyle, D., Maguire, L., Watson, D. R., & McGinnity, T. M. (2011). Gray matter concentration and effective connectivity changes in Alzheimer's disease: a longitudinal structural MRI study. *Neuroradiology*, *53*(10), 733–48. https://doi.org/10.1007/s00234-010-0795-1

Luo, Q., Lu, W., Cheng, W., Valdes-Sosa, P. A., Wen, X., Ding, M., & Feng, J. (2013). Spatio-temporal Granger causality: a new framework. *NeuroImage*, *79*, 241–63. https://doi.org/10.1016/j.neuroimage.2013.04.091

Matsuda, H. (2001). Cerebral blood flow and metabolic abnormalities in Alzheimer's disease. *Annals of Nuclear Medicine*, *15*(2), 85–92. https://doi.org/10.1007/BF02988596

Meguro, K., Blaizot, X., Kondoh, Y., Le Mestric, C., Baron, J. C., & Chavoix, C. (1999). Neocortical and hippocampal glucose hypometabolism following neurotoxic lesions of the entorhinal and perirhinal cortices in the non-human primate as shown by PET. Implications for Alzheimer's disease. *Brain*, *122*, 1519–1531. https://doi.org/10.1093/brain/122.8.1519

Meng, X., Jun, C., Wang, Q., Zhang, X., Li, Z., Li, Q., … Ma, X. (2013). High b-value diffusion tensor imaging of the remote white matter and white matter of obstructive unilateral cerebral arterial regions. *Clinical Radiology*, *68*(8), 815–22. https://doi.org/10.1016/j.crad.2013.03.009

Metzler-Baddeley, C., Hunt, S., Jones, D. K., Leemans, A., Aggleton, J. P., & O'Sullivan, M. J. (2012). Temporal association tracts and the breakdown of episodic memory in mild cognitive impairment. *Neurology*, *79*, 2233–2240. https://doi.org/10.1212/WNL.0b013e31827689e8

Metzler-Baddeley, C., Jones, D. K., Steventon, J., Westacott, L., Aggleton, J. P., & O'Sullivan, M. J. (2012). Cingulum microstructure predicts cognitive control in older age and mild cognitive impairment. *J Neurosci*, *32*(49), 17612–17619. https://doi.org/10.1523/JNEUROSCI.3299-12.2012

Mielke, M. M., Okonkwo, O. C., Oishi, K., Mori, S., Tighe, S., Miller, M. I., … Lyketsos, C. G. (2012). Fornix integrity and hippocampal volume predict memory decline and progression to Alzheimer's disease. *Alzheimer's & Dementia : The Journal of the Alzheimer's Association*, *8*(2), 105–13. https://doi.org/10.1016/j.jalz.2011.05.2416

Minka, T. P. (2001). Automatic choice of dimensionality for PCA. *Advances in Neural Information Processing Systems*, 598–604. Retrieved from papers2://publication/uuid/3CFAADF8-D881-40B7-B197-B7B3ED7391E6

Minoshima, S., Foster, N. L., & Kuhl, D. E. (1994). Posterior cingulate cortex in Alzheimer's disease. *Lancet*, *344*(8926), 895. Retrieved from http://www.ncbi.nlm.nih.gov/pubmed/7916431

Minoshima, S., Giordani, B., Berent, S., Frey, K. A., Foster, N. L., & Kuhl, D. E. (1997). Metabolic reduction in the posterior cingulate cortex in very early Alzheimer's disease. *Annals of Neurology*, *42*(1), 85–94. https://doi.org/10.1002/ana.410420114

Mintun, M. A., Larossa, G. N., Sheline, Y. I., Dence, C. S., Lee, S. Y., MacH, R. H., … Morris, J. C. (2006). [11C]PIB in a nondemented population: Potential antecedent marker of Alzheimer disease. *Neurology*, *67*, 446–452. https://doi.org/10.1212/01.wnl.0000228230.26044.a4

Moretti, D. V. (2015). Theta and alpha EEG frequency interplay in subjects with mild cognitive impairment: evidence from EEG, MRI, and SPECT brain modifications. *Frontiers in Aging Neuroscience*, *7*, 31. https://doi.org/10.3389/fnagi.2015.00031

Mormino, E. C., Smiljic, A., Hayenga, A. O., Onami, S. H., Greicius, M. D., Rabinovici, G. D., … Jagust, W. J. (2011). Relationships between β-amyloid and functional connectivity in different components of the default mode network in aging. *Cerebral Cortex (New York, N.Y. : 1991)*, *21*(10), 2399–407. https://doi.org/10.1093/cercor/bhr025

Morris, J. C., Heyman, A., Mohs, R. C., Hughes, J. P., van Belle, G., Fillenbaum, G., … Clark, C. (1989). The Consortium to Establish a Registry for Alzheimer's Disease (CERAD). Part I. Clinical and neuropsychological assessment of Alzheimer's disease. *Neurology*, *39*, 1159–1165. https://doi.org/10.1212/WNL.41.4.479

Mosconi, L., Tsui, W. H., Herholz, K., Pupi, A., Drzezga, A., Lucignani, G., … de Leon, M. J. (2008). Multicenter standardized 18F-FDG PET diagnosis of mild cognitive impairment, Alzheimer's disease, and other dementias. *Journal of Nuclear Medicine : Official Publication, Society of Nuclear Medicine*, *49*(3), 390–398. https://doi.org/10.2967/jnumed.107.045385

Mutlu, J., Landeau, B., Tomadesso, C., de Flores, R., Mézenge, F., de La Sayette, V., … Chételat, G. (2016). Connectivity disruption, atrophy, and hypometabolism within posterior cingulate networks in Alzheimer's disease. *Frontiers in Neuroscience*, *10*(DEC). https://doi.org/10.3389/fnins.2016.00582

Nestor, P. J., Fryer, T. D., Smielewski, P., & Hodges, J. R. (2003). Limbic hypometabolism in Alzheimer's disease and mild cognitive impairment. *Annals of Neurology*, *54*(3), 343–351. https://doi.org/10.1002/ana.10669

Papez, J. (1937). A proposed mechanism of emotion. *Archives of Neurology & Psychiatry*, *38*(4), 725–743. https://doi.org/10.1001/archneurpsyc.1937.02260220069003

Park, Y.-M., Che, H.-J., Im, C.-H., Jung, H.-T., Bae, S.-M., & Lee, S.-H. (2008). Decreased EEG synchronization and its correlation with symptom severity in Alzheimer's disease. *Neuroscience Research*, *62*(2), 112–7. https://doi.org/10.1016/j.neures.2008.06.009

Pasternak, O., Sochen, N., Gur, Y., Intrator, N., & Assaf, Y. (2009). Free water elimination and mapping from diffusion MRI. *Magnetic Resonance in Medicine*, *62*(3), 717–730. https://doi.org/10.1002/mrm.22055

Patel, K. T., Stevens, M. C., Pearlson, G. D., Winkler, A. M., Hawkins, K. A., Skudlarski, P., & Bauer, L. O. (2013). Default mode network activity and white matter integrity in healthy middle-aged ApoE4 carriers. *Brain Imaging and Behavior*, *7*(1), 60–67. https://doi.org/10.1007/s11682-012-9187-y

Pedro, T., Weiler, M., Yasuda, C. L., D'Abreu, A., Damasceno, B. P., Cendes, F., & Balthazar, M. L. F. (2012). Volumetric brain changes in thalamus, corpus callosum and medial temporal structures: Mild alzheimer's disease compared with amnestic mild cognitive impairment. *Dementia and Geriatric Cognitive Disorders*, *34*(3–4), 149–155. https://doi.org/10.1159/000342118

Petersen, R. C. (2004). Mild cognitive impairment as a diagnostic entity. *Journal of Internal Medicine*, *256*(3), 183–94. https://doi.org/10.1111/j.1365-2796.2004.01388.x

Petersen, R. C., Smith, G. E., Waring, S. C., Ivnik, R. J., Tangalos, E. G., & Kokmen, E. (1999). Mild cognitive impairment: clinical characterization and outcome. *Archives of Neurology*, *56*(3), 303–8. Retrieved from http://www.ncbi.nlm.nih.gov/pubmed/10190820

Pihlajamäki, M., & Sperling, R. A. (2009). Functional MRI assessment of task-induced deactivation of the default mode network in Alzheimer's disease and at-risk older individuals. *Behavioural Neurology*, *21*(1), 77–91. https://doi.org/10.3233/BEN-2009-0231

Pruessmann, K. P., Weiger, M., Scheidegger, M. B., & Boesiger, P. (1999). SENSE: Sensitivity encoding for fast MRI. *Magnetic Resonance in Medicine*, *42*, 952–962. https://doi.org/10.1002/(SICI)1522-2594(199911)42:5<952::AID-MRM16>3.0.CO;2-S

Raichle, M. E., MacLeod, A. M., Snyder, A. Z., Powers, W. J., Gusnard, D. A., & Shulman, G. L. (2001). A default mode of brain function. *Proceedings of the National Academy of Sciences of the United States of America*, *98*(2), 676–82. https://doi.org/10.1073/pnas.98.2.676

Raj, A., Kuceyeski, A., & Weiner, M. (2012). A network diffusion model of disease progression in dementia. *Neuron*, *73*(6), 1204–15. https://doi.org/10.1016/j.neuron.2011.12.040

Rami, L., Valls-Pedret, C., Bartrés-Faz, D., Caprile, C., Solé-Padullés, C., Castellvi, M., … Molinuevo, J. L. (2011). Cognitive reserve questionnaire. Scores obtained in a healthy elderly population and in one with Alzheimer's disease. *Revista de Neurologia*, *52*, 195–201. https://doi.org/rn2010478 [pii]

Roh, J. H., Qiu, A., Seo, S. W., Soon, H. W., Kim, J. H., Kim, G. H., … Na, D. L. (2011). Volume reduction in subcortical regions according to severity of Alzheimer's disease. *Journal of Neurology*, *258*(6), 1013–20. https://doi.org/10.1007/s00415-010-5872-1

Roses, A. D. (1996). Apolipoprotein E alleles as risk factors in Alzheimer's disease. *Annual Review of Medicine*, *47*, 387–400. https://doi.org/10.1146/annurev.med.47.1.387

Ryan, N. S., Keihaninejad, S., Shakespeare, T. J., Lehmann, M., Crutch, S. J., Malone, I. B., … Fox, N. C. (2013). Magnetic resonance imaging evidence for presymptomatic change in thalamus and caudate in familial Alzheimer's disease. *Brain*, *136*, 1399–1414. https://doi.org/10.1093/brain/awt065

Saalmann, Y. B., Pinsk, M. A., Wang, L., Li, X., & Kastner, S. (2012). The pulvinar regulates information transmission between cortical areas based on attention demands. *Science (New York, N.Y.)*, *337*(6095), 753–6. https://doi.org/10.1126/science.1223082

Saunders, R. C., Mishkin, M., & Aggleton, J. P. (2005). Projections from the entorhinal cortex, perirhinal cortex, presubiculum, and parasubiculum to the medial thalamus in macaque monkeys: identifying different pathways using disconnection techniques. *Experimental Brain Research*, *167*(1), 1–16. https://doi.org/10.1007/s00221-005-2361-3

Schelter, B., Winterhalder, M., & Timmer, J. (2006). Handbook of Time Series Analysis. https://doi.org/10.1002/9783527609970

Schippers, M. B., Renken, R., & Keysers, C. (2011). The effect of intra- and inter-subject variability of hemodynamic responses on group level Granger causality analyses. *NeuroImage*, *57*(1), 22–36. https://doi.org/10.1016/j.neuroimage.2011.02.008

Schreckenberger, M., Lange-Asschenfeldt, C., Lange-Asschenfeld, C., Lochmann, M., Mann, K., Siessmeier, T., … Gründer, G. (2004). The thalamus as the generator and modulator of EEG alpha rhythm: a combined PET/EEG study with lorazepam challenge in humans. *NeuroImage*, *22*(2), 637–44. https://doi.org/10.1016/j.neuroimage.2004.01.047

Sen Bhattacharya, B., Cakir, Y., Serap-Sengor, N., Maguire, L., & Coyle, D. (2013). Model-based bifurcation and power spectral analyses of thalamocortical alpha rhythm slowing in Alzheimer's Disease. *Neurocomputing*, *115*, 11–22. https://doi.org/10.1016/j.neucom.2012.10.023

Seth, A. K., Chorley, P., & Barnett, L. C. (2013). Granger causality analysis of fMRI BOLD signals is invariant to hemodynamic convolution but not downsampling. *NeuroImage*, *65*, 540–555. https://doi.org/10.1016/j.neuroimage.2012.09.049

Sheline, Y. I., Morris, J. C., Snyder, A. Z., Price, J. L., Yan, Z., D'Angelo, G., … Mintun, M. A. (2010). APOE4 allele disrupts resting state fMRI connectivity in the absence of amyloid plaques or decreased CSF Aβ42. *The Journal of Neuroscience : The Official Journal of the Society for Neuroscience*, *30*, 17035–17040. https://doi.org/10.1523/JNEUROSCI.3987-10.2010

Sheline, Y. I., Raichle, M. E., Snyder, A. Z., Morris, J. C., Head, D., Wang, S., & Mintun, M. a. (2011). Amyloid Plaques Disrupt Resting State Default Mode Network Connectivity in Cognitively Normal Elderly. *Biological Psychiatry*, *67*(6), 584–587. https://doi.org/10.1016/j.biopsych.2009.08.024.Amyloid

Sherman, S. M. (2007). The thalamus is more than just a relay. *Current Opinion in Neurobiology*, *17*(4), 417–422. https://doi.org/10.1016/j.conb.2007.07.003

Sherman, S. M., & Guillery, R. W. (2006). *Exploring the thalamus*. *San DiegoAcademic Press*. https://doi.org/10.1007/0-387-22733-4_12

Shiino, A., Watanabe, T., Maeda, K., Kotani, E., Akiguchi, I., & Matsuda, M. (2006). Four subgroups of Alzheimer's disease based on patterns of atrophy using VBM and a unique pattern for early onset disease. *NeuroImage*, *33*(1), 17–26. https://doi.org/10.1016/j.neuroimage.2006.06.010

Smith, S. M. (2002). Fast robust automated brain extraction. *Human Brain Mapping*, *17*, 143–155. https://doi.org/10.1002/hbm.10062

Smith, S. M., Miller, K. L., Salimi-Khorshidi, G., Webster, M., Beckmann, C. F., Nichols, T. E., … Woolrich, M. W. (2011). Network modelling methods for FMRI. *NeuroImage*, *54*(2), 875–891. https://doi.org/10.1016/j.neuroimage.2010.08.063

Sorg, C., Calhoun, V. D., Eichele, T., La, L., Riedl, V., Mu, M., … Fo, H. (2007). Selective changes of resting-state networks in individuals at risk for Alzheimer ' s disease. *PNAS*, *104*(47).

Stephan, B. C. M., Hunter, S., Harris, D., Llewellyn, D. J., Siervo, M., Matthews, F. E., & Brayne, C. (2012). The neuropathological profile of mild cognitive impairment (MCI): a systematic review. *Molecular Psychiatry*. https://doi.org/10.1038/mp.2011.147

Teipel, S., & Grothe, M. J. (2016). Does posterior cingulate hypometabolism result from disconnection or local pathology across preclinical and clinical stages of Alzheimer's disease? *European Journal of Nuclear Medicine and Molecular Imaging*, *43*(3), 526–536. https://doi.org/10.1007/s00259-015-3222-3

Tournier, J.-D., Calamante, F., & Connelly, A. (2012). MRtrix: Diffusion tractography in crossing fiber regions. *International Journal of Imaging Systems and Technology*, *22*(1), 53–66. https://doi.org/10.1002/ima.22005

Tournier, J.-D., Calamante, F., Gadian, D. G., & Connelly, A. (2004). Direct estimation of the fiber orientation density function from diffusion-weighted MRI data using spherical

deconvolution. *NeuroImage*, *23*(3), 1176–85. https://doi.org/10.1016/j.neuroimage.2004.07.037

Tournier, J.-D., Yeh, C.-H., Calamante, F., Cho, K.-H., Connelly, A., & Lin, C.-P. (2008). Resolving crossing fibres using constrained spherical deconvolution: validation using diffusion-weighted imaging phantom data. *NeuroImage*, *42*(2), 617–25. https://doi.org/10.1016/j.neuroimage.2008.05.002

Tournier, J. D., Calamante, F., & Connelly, A. (2007). Robust determination of the fibre orientation distribution in diffusion MRI: Non-negativity constrained super-resolved spherical deconvolution. *NeuroImage*, *35*, 1459–1472. https://doi.org/10.1016/j.neuroimage.2007.02.016

Valla, J., Berndt, J. D., & Gonzalez-Lima, F. (2001). Energy hypometabolism in posterior cingulate cortex of Alzheimer's patients: superficial laminar cytochrome oxidase associated with disease duration. *The Journal of Neuroscience : The Official Journal of the Society for Neuroscience*, *21*, 4923–4930. https://doi.org/21/13/4923 [pii]

Van Essen, D. C., Smith, S. M., Barch, D. M., Behrens, T. E. J., Yacoub, E., & Ugurbil, K. (2013). The WU-Minn Human Connectome Project: An overview. *NeuroImage*, *80*, 62–79. https://doi.org/10.1016/j.neuroimage.2013.05.041

Vann, S. D., Aggleton, J. P., & Maguire, E. A. (2009). What does the retrosplenial cortex do? *Nature Reviews. Neuroscience*, *10*, 792–802. https://doi.org/10.1038/nrn2733

Villain, N., Desgranges, B., Viader, F., de la Sayette, V., Mezenge, F., Landeau, B., … Chetelat, G. (2008). Relationships between Hippocampal Atrophy, White Matter Disruption, and Gray Matter Hypometabolism in Alzheimer's Disease. *Journal of Neuroscience*, *28*(24), 6174–6181. https://doi.org/10.1523/JNEUROSCI.1392-08.2008

Wang, D., Kong, Y., Chu, W. C. W., Tam, C. W. C., Lam, L. C. W., Wang, Y., … Shi, L. (2014). Generation of the probabilistic template of default mode network derived from resting-state fMRI. *IEEE Transactions on Bio-Medical Engineering*, *61*(10), 2550–5. https://doi.org/10.1109/TBME.2014.2323078

Wang, L., Roe, C. M., Snyder, A. Z., Brier, M. R., Thomas, J. B., Xiong, C., … Ances, B. M. (2012). Alzheimer disease family history impacts resting state functional connectivity. *Annals of Neurology*, *72*, 571–577. https://doi.org/10.1002/ana.23643

Welsh, K. A., Butters, N., Hughes, J. P., Mohs, R. C., & Heyman, A. (1992). Detection and staging of dementia in Alzheimer's disease. Use of the neuropsychological measures developed for the Consortium to Establish a Registry for Alzheimer's Disease. *Archives of Neurology*, *49*, 448–452. https://doi.org/10.1001/archneur.1992.00530290030008

Welsh, K., Butters, N., Hughes, J., Mohs, R., & Heyman, A. (1991). Detection of abnormal memory decline in mild cases of Alzheimer's disease using CERAD neuropsychological measures. *Archives of Neurology*, *48*, 278–281. https://doi.org/10.1001/archneur.1991.00530150046016

Wen, X., Rangarajan, G., & Ding, M. (2013). Is Granger Causality a Viable Technique for Analyzing fMRI Data? *PLoS ONE*, *8*(7). https://doi.org/10.1371/journal.pone.0067428

Wermke, M., Sorg, C., Wohlschläger, A. M., & Drzezga, A. (2008). A new integrative model of cerebral activation, deactivation and default mode function in Alzheimer's disease. *European Journal of Nuclear Medicine and Molecular Imaging*, *35 Suppl 1*, S12-24. https://doi.org/10.1007/s00259-007-0698-5

Wheeler-Kingshott, C. A. M., & Cercignani, M. (2009). About "axial" and "radial" diffusivities. *Magnetic Resonance in Medicine*, *61*(5), 1255–60. https://doi.org/10.1002/mrm.21965

Wiener, N. (1956). The Theory of Prediction. In *Modern Mathematics for Engineers* (Vol. 58, pp. 323–329).

Xie, S., Zuo, N., Shang, L., Song, M., Fan, L., & Jiang, T. (2015). How does B-value affect HARDI reconstruction using clinical diffusion MRI data? *PloS One*, *10*(3), e0120773. https://doi.org/10.1371/journal.pone.0120773

Xuereb, J. H., Perry, R. H., Candy, J. M., Perry, E. K., Marshall, E., & Bonham, J. R. (1991). Nerve cell loss in the thalamus in Alzheimer's disease and Parkinson's disease. *Brain : A Journal of Neurology*, *114 (Pt 3*, 1363–79. Retrieved from http://www.ncbi.nlm.nih.gov/pubmed/2065255

Yakushev, I., Schreckenberger, M., Müller, M. J., Schermuly, I., Cumming, P., Stoeter, P., … Fellgiebel, A. (2011). Functional implications of hippocampal degeneration in early Alzheimer's disease: A combined DTI and PET study. *European Journal of Nuclear Medicine and Molecular Imaging*, *38*(12), 2219–2227. https://doi.org/10.1007/s00259-011-1882-1

Yeatman, J. D., Weiner, K. S., Pestilli, F., Rokem, A., Mezer, A., & Wandell, B. a. (2014). The vertical occipital fasciculus: A century of controversy resolved by in vivo measurements. *Proceedings of the National Academy of Sciences*, *111*(48), E5214–E5223. https://doi.org/10.1073/pnas.1418503111

Yesavage, J. A., Brink, T. L., Rose, T. L., Lum, O., Huang, V., Adey, M., & Leirer, V. O. (1983). Development and validation of a geriatric depression screening scale: a preliminary report. *Journal of Psychiatric Research*, *17*(1), 37–49. Retrieved from http://www.ncbi.nlm.nih.gov/pubmed/7183759

Zarei, M., Beckmann, C. F., Binnewijzend, M. A. A., Schoonheim, M. M., Oghabian, M. A., Sanz-Arigita, E. J., … Barkhof, F. (2013). Functional segmentation of the hippocampus in the healthy human brain and in Alzheimer's disease. *NeuroImage*, *66*, 28–35. https://doi.org/10.1016/j.neuroimage.2012.10.071

Zarei, M., Patenaude, B., Damoiseaux, J., Morgese, C., Smith, S., Matthews, P. M., … Jenkinson, M. (2010). Combining shape and connectivity analysis: an MRI study of

thalamic degeneration in Alzheimer's disease. *NeuroImage*, *49*(1), 1–8. https://doi.org/10.1016/j.neuroimage.2009.09.001

Zhang, D., Snyder, A. Z., Fox, M. D., Sansbury, M. W., Shimony, J. S., & Raichle, M. E. (2008). Intrinsic functional relations between human cerebral cortex and thalamus. *Journal of Neurophysiology*, *100*(4), 1740–1748. https://doi.org/10.1152/jn.90463.2008

Zhang, D., Snyder, A. Z., Shimony, J. S., Fox, M. D., & Raichle, M. E. (2010). Noninvasive functional and structural connectivity mapping of the human thalamocortical system. *Cerebral Cortex (New York, N.Y. : 1991)*, *20*(5), 1187–94. https://doi.org/10.1093/cercor/bhp182

Zhang, Y., Brady, M., & Smith, S. (2001). Segmentation of brain MR images through a hidden Markov random field model and the expectation-maximization algorithm. *IEEE Transactions on Medical Imaging*, *20*(1), 45–57. https://doi.org/10.1109/42.906424

Zhang, Y., Schuff, N., Camacho, M., Chao, L. L., Fletcher, T. P., Yaffe, K., … Weiner, M. W. (2013). MRI markers for mild cognitive impairment: comparisons between white matter integrity and gray matter volume measurements. *PloS One*, *8*(6), e66367. https://doi.org/10.1371/journal.pone.0066367

Zhu, D. C., Majumdar, S., Korolev, I. O., Berger, K. L., & Bozoki, A. C. (2013). Alzheimer's disease and amnestic mild cognitive impairment weaken connections within the default-mode network: a multi-modal imaging study. *Journal of Alzheimer's Disease : JAD*, *34*(4), 969–84. https://doi.org/10.3233/JAD-121879

Figure 1: Regions of interest moving from inferior (top left) to superior (bottom right) defining thalamo-DMN white matter tractography masks. DMN components mPFC, MTG, IPL, and PCC were defined using probabilistic template (D. Wang et al., 2014) while thalamus and hippocampus were defined using the Harvard-Oxford subcortical structural atlas.

Figure 2: A, Significantly reduced incoming effective connectivity to left IPL from thalamus and posterior DMN nodes. B, Significantly reduced FA in thalamo-IPL tracts where the magnitude of reduction corresponded to the degree of effective connectivity disruption in A. C, Significantly reduced DA in the left Papez circuit including hippocampo-thalamus, thalamo-PCC, and PCC-hippocampal tracts. D, As in C, significantly reduced MD in the left Papez circuit. E, Significantly reduced RD in left hippocampo-PCC tracts.

Figure 3: Example thalamo-DMN white matter tracts from a single representative healthy subject.

Figure 4: A, Significant association between structural integrity of thalamo-cortical white matter pathways and memory performance in aMCI subjects. B, Significant association between inferior parietal lobe effective connectivity and memory performance in HCs.

Table 1: MMSE, mini-mental state exam; GDS, geriatric depression scale; EPQ E, Eysenck personality questionnaire extraversion scale; EPQ N, Eysenck personality questionnaire neuroticism scale; CR, cognitive reserve scale. Standard deviations are indicated. Results of independent samples t-tests, except for gender which was compared with a Fischer's exact test. Statistically significant differences are indicated in bold.

	HC (n=26)	aMCI (n=20)	p* (df=44)
Gender	15M,11F	10M,10F	1.00
Age	69.30 ± 6.35	69.05 ± 7.55	0.90
Ethnicity	White (Irish)	White (Irish)	-
Education	13.38 ± 3.73	14.32 ± 3.02	0.38
MMSE	28.65 ± 0.85	27.05 ± 2.17	**0.0013**
GDS	0.77 ± 1.07	2.58 ± 2.27	**0.0008**
EPQ E	8.04 ± 2.47	5.53 ± 3.37	**0.0061**
EPQ N	2.69 ± 2.43	3.78 ± 3.39	0.21
CR	16.65 ± 3.62	16.58 ± 4.97	0.95

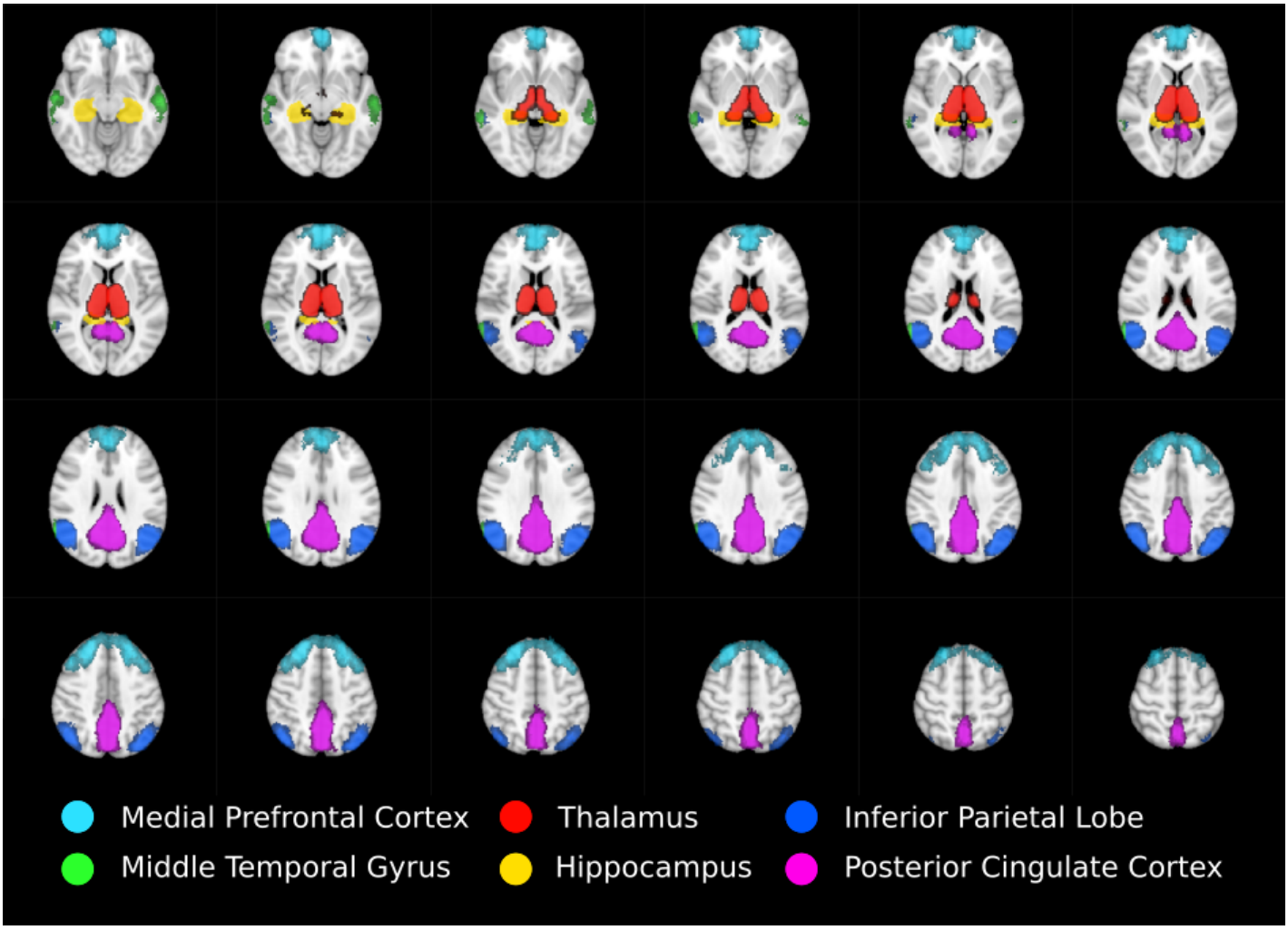
Medial Prefrontal Cortex
Thalamus
Inferior Parietal Lobe
Middle Temporal Gyrus
Hippocampus
Posterior Cingulate Cortex

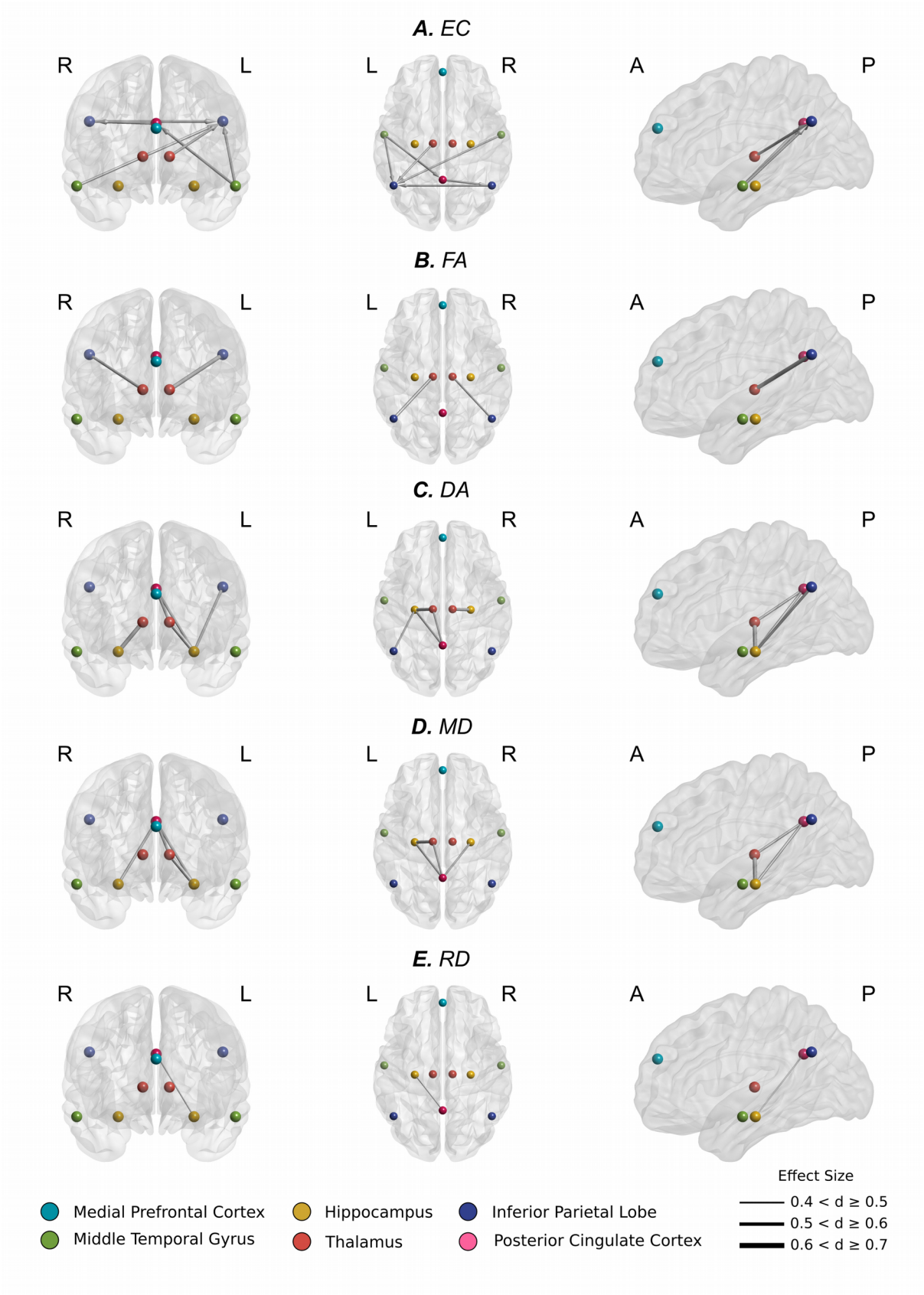
A. EC
B. FA
C. DA
D. MD
E. RD
R
L
A
P
Medial Prefrontal Cortex
Middle Temporal Gyrus
Hippocampus
Thalamus
Inferior Parietal Lobe
Posterior Cingulate Cortex
Effect Size
0.4 < d ≥ 0.5
0.5 < d ≥ 0.6
0.6 < d ≥ 0.7

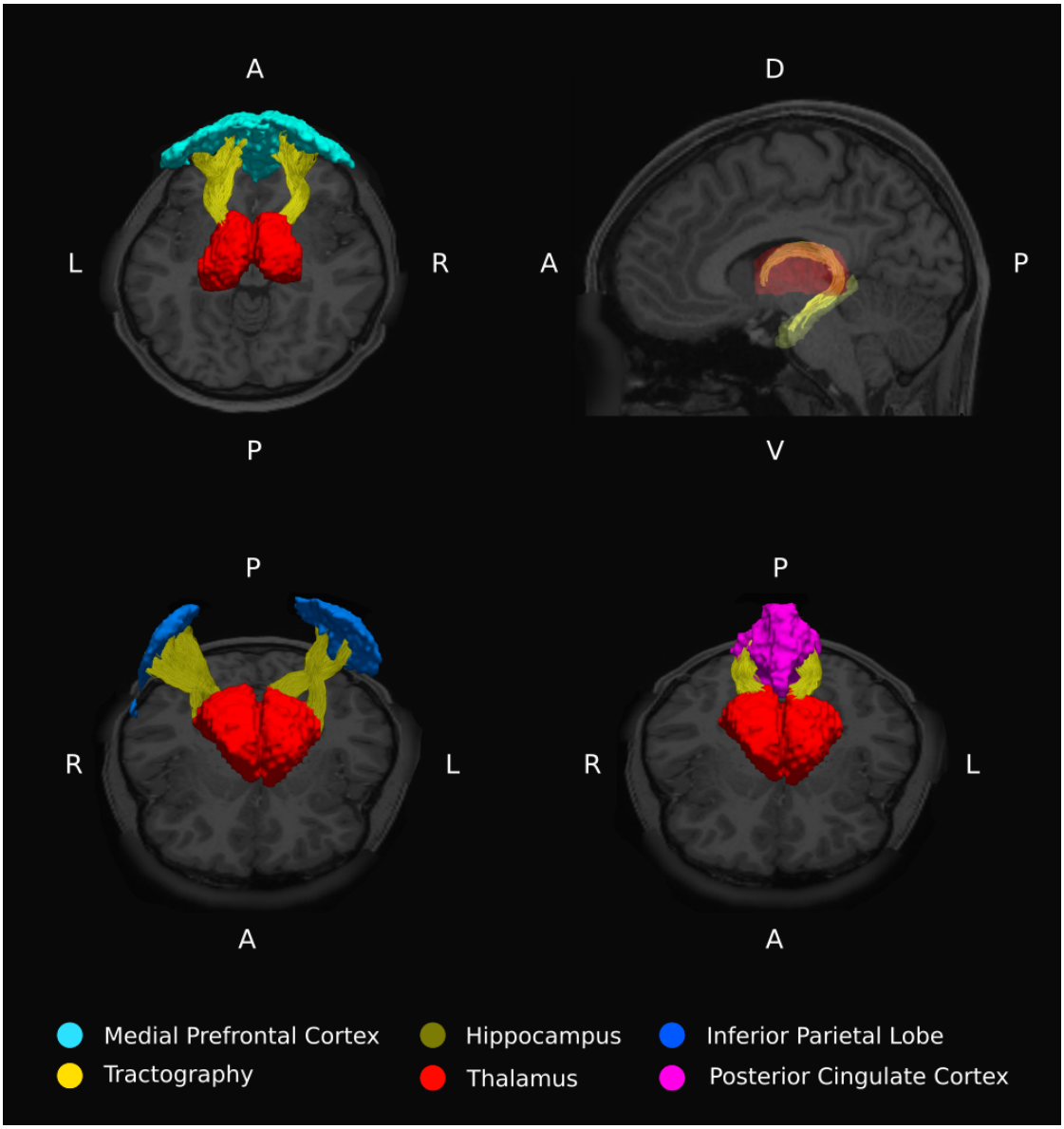
A
L
R
P
D
A
P
V
P
R
L
A
P
R
L
A
Medial Prefrontal Cortex
Tractography
Hippocampus
Thalamus
Inferior Parietal Lobe
Posterior Cingulate Cortex

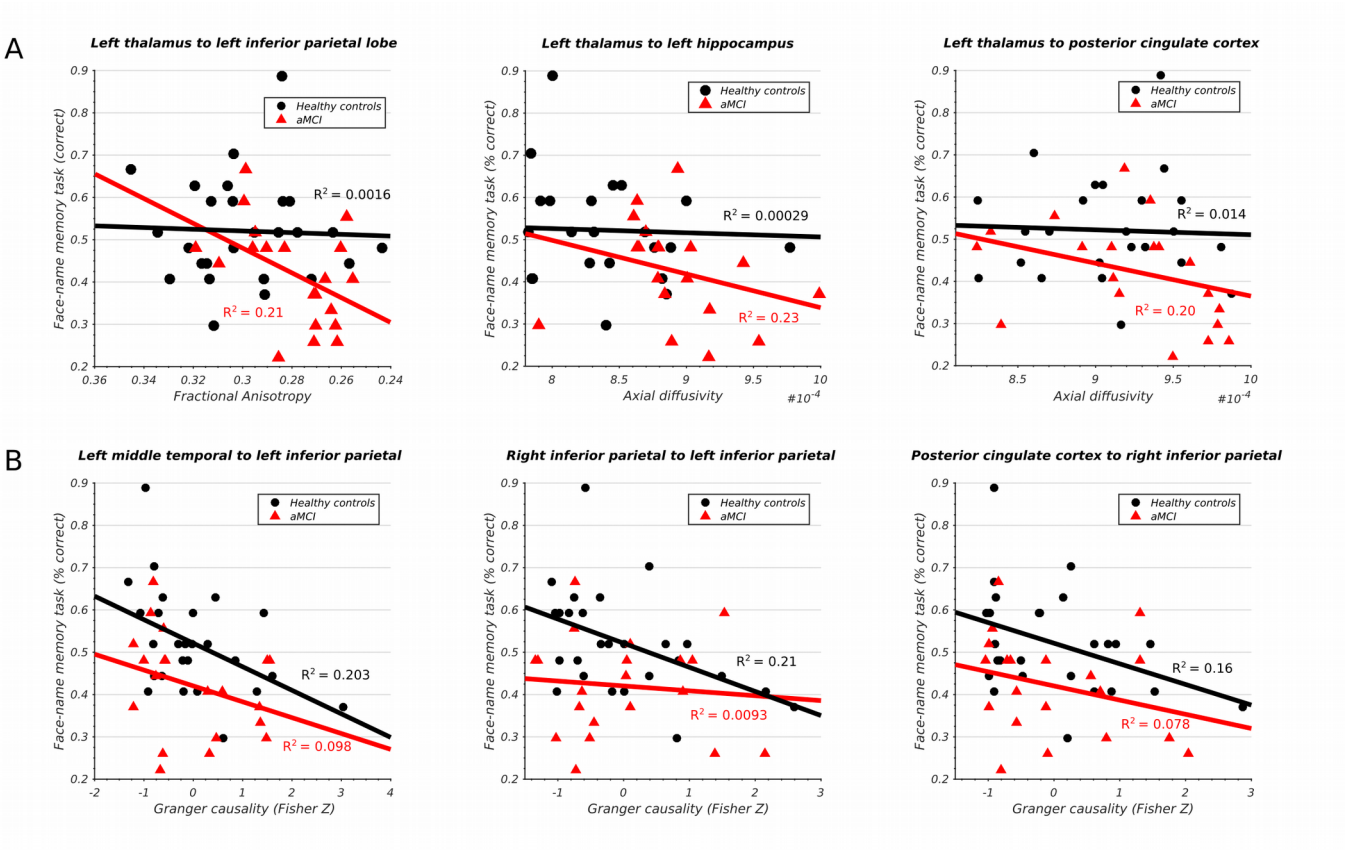
A
Left thalamus to left inferior parietal lobe
Face-name memory task (correct)
Fractional Anisotropy
Healthy controls
aMCI
R² = 0.0016
R² = 0.21
Left thalamus to left hippocampus
Face-name memory task (% correct)
Axial diffusivity
#10⁻⁴
R² = 0.00029
R² = 0.23
Left thalamus to posterior cingulate cortex
Face-name memory task (% correct)
Axial diffusivity
#10⁻⁴
R² = 0.014
R² = 0.20
B
Left middle temporal to left inferior parietal
Face-name memory task (% correct)
Granger causality (Fisher Z)
R² = 0.203
R² = 0.098
Right inferior parietal to left inferior parietal
Face-name memory task (% correct)
Granger causality (Fisher Z)
R² = 0.21
R² = 0.0093
Posterior cingulate cortex to right inferior parietal
Face-name memory task (% correct)
Granger causality (Fisher Z)
R² = 0.16
R² = 0.078